# Magnetic Polyoxometalates: Anisotropic Antiferro- and Ferromagnetic Exchange Interactions in the Pentameric Cobalt(II) Cluster $[Co_3W(D_2O)_2(CoW_9O_{34})_2]^{12-}$. A Magnetic and Inelastic Neutron Scattering Study

**Hanspeter Andres,[†] Juan M. Clemente-Juan,[‡] Reto Basler,[†] Michael Aebersold,[†] Hans-Ulrich Güdel,*[,†] Juan J. Borrás-Almenar,[‡] A. Gaita,[‡] Eugenio Coronado,*[,‡] Herma Büttner,[§] and Stefan Janssen[||]**

Departement für Chemie und Biochemie, Universität Bern, Freiestrasse 3, 3000 Bern 9, Switzerland, Departamento de Química Inorgánica, Universidad de Valencia, Dr. Moliner 50, 46100 Burjassot, Spain, Institute Laue Langevin, Avenue des Martyrs, B.P. 156, F-38042 Grenoble Cedex 9, France, and Laboratorium für Neutronenstreuung, ETH Zürich & PSI Villigen, 5232 Villigen PSI, Switzerland

*Received December 21, 2000*

The ground-state properties of the pentameric Co(II) cluster $[Co_3W(D_2O)_2(CoW_9O_{34})_2]^{12-}$ were investigated by combining magnetic susceptibility and low-temperature magnetization measurements with a detailed inelastic neutron scattering (INS) study on a fully deuterated polycrystalline sample of $Na_{12}[Co_3W(D_2O)_2(CoW_9O_{34})_2]\cdot 46D_2O$. The encapsulated magnetic $Co_5$ unit consists of three octahedral and two tetrahedral oxo-coordinated Co(II) ions. Thus, two different types of exchange interactions are present within this cluster: a ferromagnetic interaction between the octahedral Co(II) ions and an antiferromagnetic interaction between the octahedral and the tetrahedral Co(II) ions. As a result of the single-ion anisotropy of the octahedral Co(II) ions, the appropriate exchange Hamiltonian to describe the ground-state properties of the $Co_5$ spin cluster is anisotropic and is expressed as $\hat{H} = -2\sum_{i=x,y,z} J_{1i}[\hat{S}_{1i}\hat{S}_{2i} + \hat{S}_{2i}\hat{S}_{3i}] + J_{2i}[\hat{S}_{1i}\hat{S}_{5i} + \hat{S}_{2i}\hat{S}_{5i} + \hat{S}_{2i}\hat{S}_{6i} + \hat{S}_{3i}\hat{S}_{6i}]$, where $J_{1i}$ are the components of the exchange interaction between the octahedral Co(II) ions and $J_{2i}$ are the components of the exchange interaction between the octahedral and tetrahedral Co(II) ions (see Figure 1d). The study of the exchange interactions in the two structurally related polyoxoanions $[Co_4(H_2O)_2(PW_9O_{34})_2]^{10-}$ and $[Co_3W(H_2O)_2(ZnW_9O_{34})_2]^{12-}$ allowed an independent determination of the ferromagnetic exchange parameters $J_{1x} = 0.70$ meV, $J_{1y} = 0.43$ meV, and $J_{1z} = 1.51$ meV (set a) and $J_{1x} = 1.16$ meV, $J_{1y} = 1.16$ meV and $J_{1z} = 1.73$ meV (set b), respectively. Our analysis proved to be much more sensitive to the size and anisotropy of the antiferromagnetic exchange interaction $J_2$. We demonstrate that this exchange interaction exhibits a rhombic anisotropy with exchange parameters $J_{2x} = -1.24$ meV, $J_{2y} = -0.53$ meV, and $J_{2z} = -1.44$ meV (set a) or $J_{1x} = -1.19$ meV, $J_{1y} = -0.53$ meV, and $J_{1z} = -1.44$ meV (set b). The two parameter sets reproduce in a satisfactory manner the susceptibility, magnetization, and INS properties of the title compound.

## 1. Introduction

Polyoxometalates are a rich class of inorganic compounds with a remarkable degree of molecular and electronic tunabilities that have impact in disciplines as diverse as catalysis, medicine, and materials science.[1,2] They prove especially valuable for the study of magnetic interactions in clusters because many of these structures permit the inclusion of well-isolated clusters of paramagnetic ions with various nuclearities and definite topologies and geometries.[3] A good example of this ability is provided by the complexes obtained from the lacunary trivacant Keggin ligands $[PW_9O_{34}]^{9-}$ and divalent paramagnetic transition-metal ions. In these, a large diversity of magnetic clusters with nuclearities 3, 4, and 9 can be created with ferromagnetic interactions resulting in high-spin multiplicities, as well as antiferromagnetic clusters with spin frustration and clusters with competing ferro- and antiferromagnetic interactions.[4−9]

Information about the exchange interactions in clusters of transition-metal ions is usually derived from the temperature dependence of the magnetic susceptibility. This requires a model fit to the experimental data and leads to values of the exchange parameters. The danger in this procedure lies in the low information content of the susceptibility versus temperature data, which often does not allow a discrimination between physically different models. Especially when the size of the cluster gets bigger and, in addition, anisotropy becomes im-

[†] Universität Bern.
[‡] Universidad de Valencia.
[§] Institute Laue Langevin.
[||] Laboratorium für Neutronenstreuung.

(1) An updated revision of the state of the art in this burgeoning subarea of chemistry can be found in this special thematic issue: *Chem. Rev.* **1998**, *98*, 1−390.
(2) Pope, M. T.; Müller, A. *Polyoxometalates: From Platonic Solids to Anti-Retroviral Activity*; Kluwer Academic Publishers: Dordrecht, The Netherlands, 1994.
(3) Clemente-Juan, J. M.; Coronado, E. *Coord. Chem. Rev.* **1999**, *193*−*195*, 361−394.
(4) Gómez-García, C. J.; Coronado, E.; Ouahab, L. *Angew. Chem., Int. Ed. Engl.* **1992**, *31*, 240.
(5) Gómez-García, C. J.; Coronado, E.; Borrás-Almenar, J. J. *Inorg. Chem.* **1992**, *31*, 1667.
(6) Casañ-Pastor, N.; Bas, J.; Coronado, E.; Pourroy, G.; Baker, L. C. W. *J. Am. Chem. Soc.* **1992**, *114*, 10380.
(7) Gómez-García, C. J.; Coronado, E.; Gómez-Romero, P.; Casañ-Pastor, N. *Inorg. Chem.* **1993**, *32*, 3378.
(8) Galán, J. R.; Gómez-García, C. J.; Borrás-Almenar, J. J.; Coronado, E. *Adv. Mater.* **1994**, *6*, 221.
(9) Clemente, J. M.; Coronado, E.; Galán-Mascaros, J. R.; Gómez-García, C. J. *Inorg. Chem.* **1999**, *38*, 55.

10.1021/ic001437a CCC: $20.00 © 2001 American Chemical Society
Published on Web 03/16/2001

portant, a susceptibility curve does not contain enough information to determine the relevant interaction parameters, so a combination of several techniques is needed. Our approach to the energy splitting resulting from the exchange interaction is a more direct one. By using spectroscopic techniques, we try to determine these splittings independent of any theoretical model. In a second step the experimentally determined energy-level pattern is then reproduced by the eigenvalues of an appropriate effective spin Hamiltonian. The experimental technique employed is inelastic neutron scattering (INS), which has proved to be valuable in the study of transition and rare-earth metal ion clusters.[10,11] However, relatively few examples have been studied so far, most of them dimers or isotropic exchange systems with higher nuclearity. The first example, in which a single-ion anisotropy was taken into account, was a Ni(II) dimer.[12] Anisotropy was also considered in various rare-earth and mixed rare-earth/transition-metal dimers.[13−16] For higher nuclearity clusters we should mention a $Cr(III)_4$ cluster with rhombuslike geometry,[17,18] a $Ti(II)[Mn(II)]_6$ cluster,[19] an $Fe(III)_6$ wheel[20,21] as well as an $Fe(III)_8$,[22] and a $Mn(III,IV)_4$[23] and a $Mn(III,IV)_{12}$ acetate[24,25] cluster. In the last three examples INS was used to obtain information on the zero-field splitting (ZFS) within the cluster ground states.

More recently we have also applied this technique to study the more complex high-nuclearity magnetic clusters furnished by polyoxometalate chemistry.[26−29] INS provided a clear answer to the nature of the magnetic coupling in the Keggin derivative $K_8[Co_2(D_2O)(W_{11}O_{39})]\cdot nD_2O$ (short $Co_2$).[30,31] The structure is shown in Figure 1a. The embedded magnetic $Co_2$ unit is shown in black. The Co(II) dimer consists of a tetrahedral and an octahedral oxo-coordinated Co(II) ion sharing a corner oxygen. The octahedral Co(II) ion possesses a considerable orbital moment in the electronic $^4T_1$ ground state, which should result in an anisotropic exchange coupling. Whereas the magnetic susceptibility has been interpreted in terms of a Heisenberg coupling model,[32] we have clearly shown by INS that the coupling is highly anisotropic.[27] In the polyoxometalate series $[M_4(H_2O)_2(PW_9O_{34})_2]^{10-}$ (short $M_4$; M = Mn(II), Fe(II), Co(II), Ni(II), and Cu(II))[4−8] we studied the embedded magnetic $M_4$ unit of the Ni(II) and Co(II) species by means of INS.[9,28,29] The edge-sharing $MO_6$ octahedra are depicted in black in Figure 1c. In the Ni(II) analogue INS has shown that the isotropic Heisenberg model supplemented by a second-order single-ion ZFS term is the appropriate spin Hamiltonian for the description of the ground-state properties of this rhombuslike cluster.[28] The bulk magnetic susceptibility provided the information about the sign of the exchange interactions but was shown to be largely insensitive to their values, in particular to the pairwise interaction along the diagonal of the rhomb. Whereas magnetization measurements enabled the determination of a mean ZFS parameter *D*, INS allowed us to distinguish between the distortions in the two different Ni(II) sites. The real strength of INS became manifest in the study of the Co(II) tetramer, where the anisotropy has its origin in a first-order spin−orbit coupling.[9,29] Whereas the overall ferromagnetic nature of the exchange coupling is derived from the susceptibility, the size and the anisotropy of the two competing exchange interactions along the edges and the diagonal of the rhombus could only be determined by INS. The experimentally derived ground-state splitting was very well reproduced by an exchange Hamiltonian with axial anisotropy.[9] But the drop of the assumption of axial anisotropy was essential to reproduce the observed INS intensities and their dependence on the scattering vector $\vec{Q}$.[29]

The structure of the title compound is shown in Figure 1d. The white octahedra contain a central W atom, whereas the black polyhedra contain an oxo-coordinated Co(II) ion. The embedded magnetic $Co_5$ spin cluster comprises two tetrahedral and three octahedral Co(II) ions. This results in the presence of two competing anisotropic ferro- and antiferromagnetic exchange

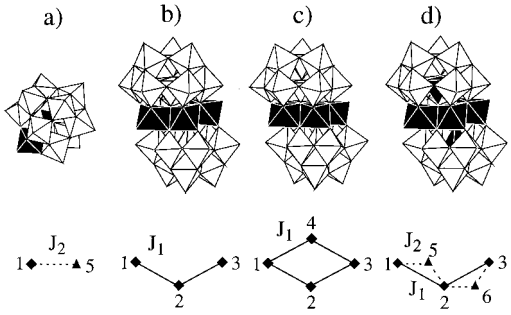


**Figure 1.** Top: Structures of the polyoxometalates $[Co_2(H_2O)(W_{11}O_{39})]^{8-}$ (a), $[Co_3W(H_2O)_2(ZnW_9O_{34})_2]^{12-}$ (b), $[Co_4(H_2O)_2(PW_9O_{34})_2]^{10-}$ (c), and $[Co_3W(H_2O)_2(CoW_9O_2)]^{12-}$ (d). The white polyhedra contain an oxo-coordinated W, P, or Zn(II) ion, whereas the black polyhedra contain an oxo-coordinated Co(II) ion in the central position. Bottom: Exchange networks of the corresponding magnetic clusters. Octahedral and tetrahedral oxo-coordinated Co(II) ions are shown as black diamonds and triangles, respectively. The exchange pathways $J_1$ and $J_2$ are depicted as full and dotted lines, respectively.

(10) Furrer A.; Güdel, H. U. *Phys. Rev. Lett.* **1977**, *39*, 657.
(11) Güdel H. U. In *Molecular Magnetism: From Molecular Assemblies to Devices*; Coronado, E., Delhás, P., Gatteschi, D., Miller, J. S., Eds.; NATO ASI Series E321; Kluwer Academic Publishers: Dordrecht, The Netherlands, 1996; pp 229−242.
(12) Stebler, A.; Güdel, H. U.; Furrer, A.; Kjems, J. K. *Inorg. Chem.* **1982**, *21*, 380.
(13) Güdel, H. U.; Furrer, A.; Kjems, J. K. *Inorg. Chem.* **1990**, *21*, 4081.
(14) Furrer, A.; Güdel, H. U.; Krausz, E. R.; Blank, H. *Phys. Rev. Lett.* **1990**, *64*, 68.
(15) Aebersold, M.; Güdel, H. U.; Hauser, A.; Furrer, A.; Blank, H.; Kahn, R. *Phys. Rev. B* **1993**, *73*, 12723.
(16) Güdel, H. U. *Neutron News* **1996**, *73*, 24.
(17) Furrer, A.; Güdel, H. U.; Hauser, U. *J. Appl. Phys.* **1979**, *50*, 2043.
(18) Güdel, H. U.; Hauser, U.; Furrer, A. *Inorg. Chem.* **1979**, *18*, 2730.
(19) Aebersold, M.; Blank, H.; Briat, B.; Furrer, A.; Güdel, H. U. *Inorg. Chem.* **1991**, *30*, 3280.
(20) Waldmann, O.; Schülein, J.; Koch, R.; Müller, P.; Bernt, I.; Saalfrank, R. W.; Andres, H.; Güdel, H. U.; Allenspach, P. *Inorg. Chem.* **1999**, *38*, 5879.
(21) Andres, H. P.; Güdel, H. U.; Bernt, I.; Saalfrank, R. W.; Allenspach, P. *Swiss Neutron News* **1999**, *15*, 15.
(22) Carciuffo, R.; Amoretti, G.; Murani, A.; Sessoli, R.; Caneschi, A.; Gatteschi, D. *Phys. Rev. Lett.* **1998**, *81*, 4744.
(23) Andres, H. P.; Basler, R.; Güdel, H. U.; Aromí, G.; Christou, G.; Büttner, H.; Rufflé, B. *J. Am. Chem. Soc.* **2000**, *122*, 12469−12477.
(24) Hennion, M.; Pardi, L.; Mirebeau, I.; Suard, E.; Sessoli, R.; Caneschi, A. *Phys. Rev. B* **1997**, *56*, 8819.
(25) Mirebeau, I.; Hennion, M.; Casalta, H.; Andres, H.; Güdel, H. U.; Irodova, A. V.; Caneschi, A. *Phys. Rev. Lett.* **1999**, *83*, 628.
(26) Clemente, J. M.; Andres, H. P.; Aebersold, M.; Borras-Almenar, J. J.; Coronado, E.; Güdel, H. U.; Büttner, H.; Kearly, G. *Inorg. Chem.* **1997**, *36*, 2244.
(27) Andres, H.; Aebersold, M.; Güdel, H. U.; Clemente-Juan, J. M.; Coronado, E.; Büttner, H.; Kearly, G.; Zolliker, M. *Chem. Phys. Lett.* **1998**, *289*, 224.
(28) Clemente-Juan, J. M.; Andres, H.; Borrás-Almenar, J. J.; Coronado, E.; Güdel, H. U.; Aebersold, M.; Kearly G.; Büttner, H. J. *Am. Chem. Soc.* **1999**, *121*, 10021−10027.
(29) Andres, H.; Clemente-Juan, J. M.; Aebersold, M.; Güdel, H. U.; Coronado, E.; Büttner, H.; Kearly, G.; Melero, J.; Burriel, R. *J. Am. Chem. Soc.* **1999**, *121*, 10028−10034.
(30) Baker, L. C. W.; McCutcheon, T. P. *J. Am. Chem. Soc.* **1956**, *78*, 4503.
(31) Baker, L. C. W.; Baker, S. W.; Eriks, K.; Pope, M. T.; Shibata, M.; Rollins, O. W.; Fang, J. H.; Koh, L. L. *J. Am. Chem. Soc.* **1966**, *88*, 2329.
(32) Baker, L. C. W.; Baker, V. E. S.; Washfi, S. H.; Candela, G. A.; Kahn, A. H. *J. Chem. Phys.* **1972**, *56*, 4917.

interactions. Here, we tackle this problem by combining magnetic measurements with a high-resolution INS study on a fully deuterated sample of $Na_{12}[Co_3W(D_2O)_2(CoW_9O_{34})_2]\cdot 46D_2O$. Magnetically this cluster may be viewed as containing elements of both the $Co_2$ and $Co_4$ spin clusters. We make use of these earlier results and new results on a third structurally related polyoxoanion $[Co_3W(H_2O)_2(ZnW_9O_{34})_2]^{12-}$ to obtain initial values for the exchange parameters. We will show that this is indeed necessary to model the experimental data, and differences in the exchange parameters will be correlated with structural changes.

## 2. Experimental Section

An amount of approximately 20 g of $Na_{12}[Co_3W(H_2O)_2(CoW_9O_{34})_2]\cdot 46H_2O$ (short $Co_5$) and a few grams of $Na_{12}[Co_3W(H_2O)_2(ZnW_9O_{34})_2]\cdot 46H_2O$ (short $Co_3$) were obtained by the preparation described in the literature.[33] The $Co_5$ product was subsequently twice recrystallized from $D_2O$. The deuterated product was characterized by chemical analysis and X-ray powder diffraction using the program LAZY PULVERIX[34] and the structure information from the isostructural compound $Na_{12}[Zn_3W(H_2O)_2(ZnW_9O_{34})_2]\cdot 46H_2O$ in ref 33. The polycrystalline sample was then sealed under helium in an aluminum container of 15 mm diameter and 55 mm length suitable for INS experiments.

**Magnetic Measurements**. Variable-temperature susceptibility measurements were carried out in the temperature range 2−300 K at a magnetic field of 0.1 T using a magnetometer (Quantum Design MPMS-XL-5) equipped with a SQUID sensor. The data were corrected for the diamagnetic contribution, which was estimated from Pascal's constants. Isothermal magnetization measurements at low temperature (2 and 5 K) were performed up to a field of 5 T in the same apparatus.

**Inelastic Neutron Scattering**. INS spectra with cold neutrons were recorded on the time-of-flight spectrometer IN5 at the Institute Laue Langevin (ILL) in Grenoble. The measurements were performed at temperatures of 1.5, 10, and 30 K with incident neutron wavelengths of 4.2 and 5.0 Å.

INS measurements with cold neutrons in an extended dynamical range were done on the time-of-flight instrument FOCUS at the Paul Scherrer Institut (PSI) in Villigen. The spectra were recorded at a temperature of 1.5 K with incident neutron wavelengths of 2.79 and 2.92 Å.

The data treatment involved the subtraction of a background spectrum using an empty aluminum container of the same size and the calibration of the detectors by means of a spectrum of vanadium metal. The time-of-flight to energy conversion and the data reduction were done with the standard programs INX and NINX at the ILL and PSI, respectively. Further data treatment was done using the commercial program IgorPro 3.15 (Wave Metrics).

## 3. Results

**Magnetic Measurements.** Magnetic susceptibility measurements of polycrystalline samples of $Na_{12}[Co_3W(H_2O)_2(ZnW_9O_{34})_2]\cdot 46H_2O$ and $Na_{12}[Co_3W(D_2O)_2(CoW_9O_{34})_2]\cdot 46D_2O$ are shown in Figures 2a and 3a, respectively. The products $\chi T$ versus $T$ are depicted with open circles in the temperature range 2−50 K. When the samples are cooled from room temperature, the $\chi T$ product of $Co_3$ shows a small decrease from ∼10 emu K mol$^{-1}$ at 293 K to 8.8 emu K mol$^{-1}$ at 50 K where a round minimum is observed. This decrease is due to the spin−orbit coupling of Co(II). Below 50 K, $\chi T$ increases to reach a maximum of 12.8 emu K mol$^{-1}$ at 4 K. This behavior is indicative of ferromagnetic Co(II)−Co(II) interactions within the $Co_3$ spin cluster. In contrast, the magnetic behavior of $Co_5$ shows a continuous decrease in $\chi T$ upon cooling, from a value of 9.36 emu K mol$^{-1}$ at 50 K down to a value of 1.64 emu K mol$^{-1}$ at 2 K.

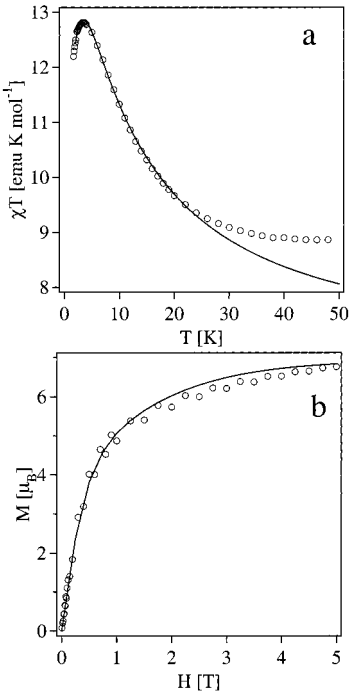


**Figure 2.** (a) Measured magnetic susceptibility of a polycrystalline sample of $Na_{12}[Co_3W(H_2O)_2(ZnW_9O_{34})_2]\cdot 46H_2O$ between 2 and 50 K depicted with open circles. (b) Isothermal magnetization of $Na_{12}[Co_3W(H_2O)_2(ZnW_9O_{34})_2]\cdot 46H_2O$ at 2 K. The solid lines represent the calculated magnetic properties when applying the Hamiltonian in eq 1 with the parameter sets in eq 7 and $g_{\parallel} = 6.43$ and $g_{\perp} = 3.82$.

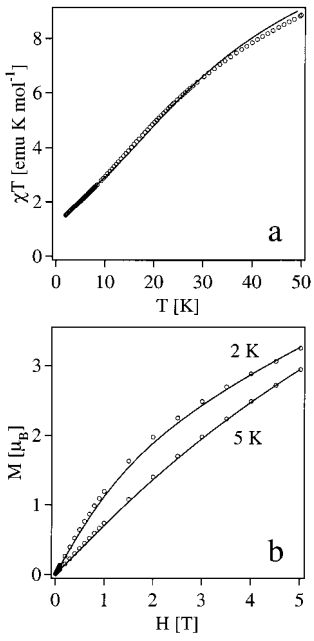


**Figure 3.** (a) Measured magnetic susceptibility of a polycrystalline sample of $Na_{12}[Co_3W(D_2O)_2(CoW_9O_{34})_2]\cdot 46D_2O$ between 2 and 50 K depicted with open circles. (b) Isothermal magnetization of $Na_{12}[Co_3W(D_2O)_2(CoW_9O_{34})_2]\cdot 46D_2O$ at 2 and 5 K. The solid lines represent the magnetic properties when applying the Hamiltonian in eq 2 with the parameter sets in eqs 5 and 6 or eqs 7 and 8 and $g_{\parallel} = 5.3$, $g_{\perp} = 7.3$ for the octahedral and $g = 2.6$ for the tetrahedral Co(II) ions.

This behavior is indicative of dominant antiferromagnetic Co(II)−Co(II) interactions within the $Co_5$ spin cluster. The field dependencies of the low-temperature isothermal magnetization are plotted for both compounds $Co_3$ and $Co_5$ in Figures 2b and 3b, respectively.

(33) Tourné, C. M.; Tourné, G. F.; Zonnevijlle, F. J. *Chem. Soc., Dalton. Trans.* **1991**, 143.
(34) Yvon, K.; Jeitschko, W.; Erwin, P. J. *Appl. Crystallogr.* **1977**, 10.

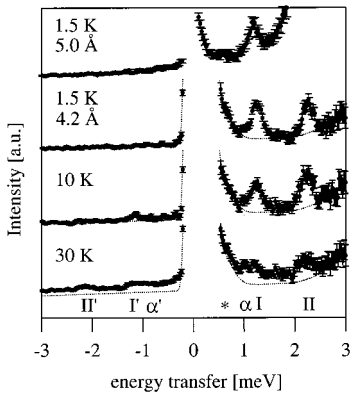


**Figure 4.** INS spectra of a polycrystalline sample of $Na_{12}[Co_3W(D_2O)_2(CoW_9O_{34})_2]\cdot 46D_2O$ recorded on IN5 at $\lambda_i = 4.2$ Å for temperatures $T = 1.5$, 10, and 30 K and for $\lambda = 5.0$ Å at $T = 1.5$ K. The peaks are labeled at the bottom of the figure. The dashed lines in the spectra represent a convolution of the experimental background and the elastic peak features.

**Inelastic Neutron Scattering.** In Figure 4 we report the INS spectra of a polycrystalline sample of $Na_{12}[Co_3W(D_2O)_2(CoW_9O_{34})_2]\cdot 46D_2O$ obtained on IN5 with an incident neutron wavelength of 4.2 Å for three temperatures. The energy-transfer range between −3 and 3 meV is depicted with positive values for neutron-energy loss. The resolution is 110 $\mu$eV at the elastic peak position. At 1.5 K we observe two prominent inelastic transitions at 1.243(8) and 2.256(7) meV on the neutron-energy loss side, labeled I and II, respectively. Below 0.8 meV the spectrum is obscured by a spurious shoulder, most probably a Bragg reflection of the aluminum-shielded cryostat. It is marked with an asterisk in the figure. An increase of the temperature to 10 and 30 K is concomitant with the appearance of a hot shoulder on the low-energy side of transition I at 1.04(3) meV, labeled α, and a decrease of the scattering intensity of transitions I and II. On the neutron-energy gain side in Figure 4 all these transitions are observed as broad features at elevated temperatures. The temperature dependence of the three bands labeled I′, II′, and α′ on the gain side is in excellent agreement with the assignment of the corresponding cold and hot transitions I, II, and α, respectively. The top spectrum in Figure 4 depicts the INS spectrum obtained with an incident neutron wavelength of $\lambda = 5.0$ Å and a temperature $T = 1.5$ K on IN5. The masked region in the 4.2 Å spectrum is now resolved, and no transition below 1 meV is observed. The results of a least-squares fitting analysis of the 1.5, 10, and 30 K spectra with Gaussians and the depicted backgrounds in Figure 4 are summarized in Table 1.

In Figure 5 the INS spectrum of $Na_{12}Co_3W(D_2O)_2(CoW_9O_{34})_2]\cdot 46D_2O$ at $\lambda_i = 2.79$ Å and $T = 1.5$ K is shown. We observe a well-resolved transition at 3.806(6) meV, labeled III. The high resolution of 155 $\mu$eV has been achieved by using the (004) reflection of pyrolytic graphite for wavelength selection and an inelastic time-focusing at 3 meV. In the inset of Figure 5 the survey spectrum between −2 and 6 meV is depicted. The higher experimental resolution of band III compared to bands I and II illustrates the effect of the inelastic time-focusing. Transition I is only observed as a shoulder of the elastic peak, whereas transition II is partially resolved. We can thus determine the intensity ratio of transition II to transition III. The resulting intensities of the least-squares fitting analysis with two Gaussians and a linear background are included in Table 1. Above 4.5 meV the spectrum measured with 2.79 Å is obscured by a broad instrumental artifact, which is not present with $\lambda_i = 2.92$ Å (data not shown). With the latter wavelength the resolution is 0.5 meV, and the INS spectrum revealed unresolved magnetic intensity, denoted as band IV, between 3.5 and 6.5 meV on the neutron-energy loss side.

The good statistics of the 1.5 K spectrum at 4.2 Å enabled us to study the behavior of the scattering intensity of transitions I and II as a function of $Q$ at five discrete points between 0.5 and 2.3 Å$^{-1}$. The result is plotted in Figure 6a with full and open circles for transitions I and II, respectively. The $Q$ dependence of transition III as obtained from the 2.79 Å data is shown with open squares for four discrete points between 0.9 and 3.4 Å$^{-1}$ in Figure 6b. The general decrease of the scattering intensity above $Q = 1$ Å$^{-1}$ identifies transitions I−III as magnetic; phonon excitations would typically show an increase of the INS intensity proportional to $Q^2$.

From the experimental data presented in Figures 4 and 5 and Table 1, we derive the energy-level diagram depicted in Figure 7. The cold transitions I−IV originating in the pentamer ground level are shown with full arrows. The hot transitions originating from the excited levels at 1.243 and 2.256 meV are shown with broken arrows. Above 4.3 meV the unresolved magnetic intensity is indicated as a gray band.

## 4. Analysis and Discussion

In the first step we elucidate the magnetic properties of the $Co_3$ spin cluster. The structure is shown in Figure 1b with the edge-sharing $CoO_6$ octahedra depicted in black. The presented magnetic data in Figure 2 are fitted to a model that considers anisotropic exchange interactions between the magnetic Co(II) ions. This anisotropy has already been encountered in the related polyoxometalate $Co_4$.[29] It arises from the electronic ground state of high-spin octahedral Co(II) ions, $^4T_1$, which splits into six Kramers doublets by spin−orbit coupling and the low-symmetry crystal field.[35] This splitting is about 50 meV, so in the temperature range 1.5−30 K only the lowest Kramers doublet is significantly populated. This Kramers doublet is well described by an anisotropic $S = {}^1/_2$ spin state. In the case of the trimer depicted in Figure 1b, the exchange Hamiltonian that describes the exchange interactions between these effective spins is written as

$$\hat{H} = -2 \sum_{i=x,y,z} J_{1i}(S_{1i}S_{2i} + S_{2i}S_{3i}) \qquad (1)$$

The exchange parameters $J_{1x} = J_{1y} = 1.16$ meV, $J_{1z} = 1.73$ meV and $g$ values of $g_{||} = 6.43$ and $g_{\perp} = 3.82$ for the three Co(II) ions provide an excellent description of the magnetic susceptibility (see Figure 2a). Above 30 K there is a deviation of the calculated susceptibility from the experimental data, which we ascribe to a population of higher Kramers doublets of the octahedral Co(II) ions. The field dependence of the low-temperature magnetization data is equally well reproduced with the same set of parameters (see Figure 2b).

It is to be noted that the simplicity of the present system, that it only involves one kind of exchange interaction, has allowed us to get useful information on the size and anisotropy of the ferromagnetic exchange interaction $J_1$. The magnetic simplicity of the magnetic $Co_3$ unit is in sharp contrast to the complexity of the exchange coupling in the title compound. This results in an overparametrization of the problem that prevents us from obtaining a reliable solution from the information content of the magnetic susceptibility. In fact, many sets of parameters are able to reproduce the magnetic behavior. Hence,

(35) Carlin, R. L. *Magnetochemistry*; Springer: Berlin, 1986.

**Table 1.** Experimentally Determined Energies and Intensities with Estimated Errors of the Various INS Transitions for Neutron-Energy Loss

| | | | intensity [arbitrary units] | | | | | | | |
|---|---|---|---|---|---|---|---|---|---|---|
| | energy [meV] | | 1.5 K | | 10 K | | 30 K | | | |
| label | exptl | calcd | exptl | calcd | exptl | calcd | exptl | calcd | $\lambda$ [c] [Å] | $Q$ range [Å$^{-1}$] |
| I | 1.243(8) | 1.244[a]<br>1.238[b] | 1.00(7) | 1.00[a]<br>1.00[b] | 0.73(7) | 0.77[a]<br>0.75[b] | 0.33(7) | 0.26[a]<br>0.26[b] | 4.2 | 0.28−2.50 |
| II | 2.256(7) | 2.259[a]<br>2.260[b] | 0.77(4) | 0.80[a]<br>0.76[b] | 0.73(7) | 0.64[a]<br>0.57[b] | 0.26(7) | 0.21[a]<br>0.20[b] | 4.2 | 0.28−2.50 |
| α | 1.04(3) | 1.02[a]<br>1.02[b] | 0.0(1) | 0.0[a]<br>0.0[b] | 0.25(1) | 0.20[a]<br>0.09[b] | 0.29(4) | 0.19[a]<br>0.09[b] | 4.2 | 0.28−2.50 |
| II | | | 1.0(3) | 1.0[a]<br>1.0[b] | | | | | 2.79 | 0.49−4.11 |
| III | 3.806(6) | 3.813[a]<br>3.807[b] | 0.3(2) | 0.1[a]<br>0.1[b] | | | | | 2.79 | 0.49−4.11 |
| IV | 4.3−6.5 | 4.3−6.4[a]<br>4.3−6.4[b] | | | | | | | 2.92 | 0.47−3.93 |

[a] Calculated energies (eq 2) and intensities (eq 10), using the following parameters: $J_{1x} = 0.70$ meV, $J_{1y} = 0.43$ meV, $J_{1z} = 1.51$ meV, $J_{2x} = -1.24$ meV, $J_{2y} = -0.53$ meV, and $J_{2z} = -1.44$ meV. [b] Calculated energies (eq 2) and intensities (eq 10), using the following parameters: $J_{1x} = 1.16$ meV, $J_{1y} = 1.16$ meV, $J_{1z} = 1.73$ meV, $J_{2x} = -1.19$ meV, $J_{2y} = -0.53$ meV, and $J_{2z} = -1.44$ meV are given for comparison. [c] For the $\lambda = 4.2$ Å experiment, the experimental and calculated intensities are scaled to the intensity of transition I at $T = 1.5$ K, whereas for the $\lambda = 2.79$ Å experiment they are scaled to transition II at $T = 1.5$ K.

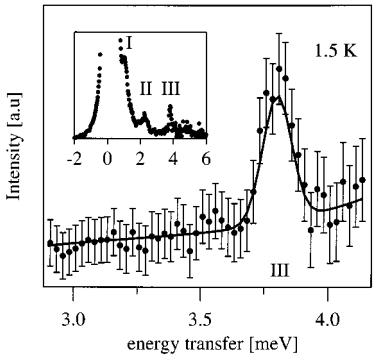


**Figure 5.** INS spectrum of a polycrystalline sample of $Na_{12}[Co_3W(D_2O)_2(CoW_9O_{34})_2]\cdot 46D_2O$ recorded on FOCUS at $\lambda_i = 2.79$ Å for a temperature $T = 1.5$ K in the energy-transfer range 2.8−4.2 meV. The inset depicts the survey spectrum between −2 and 6 meV. The peaks are labeled as in Figure 4.

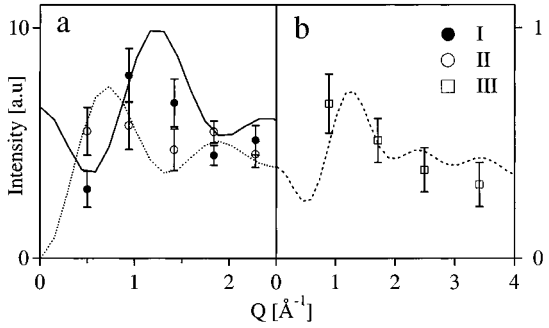


**Figure 6.** Experimental and calculated $Q$ dependencies (eq 10) of the INS intensities of transitions I and II (a) and III (b), respectively. The experimental intensities of transition III are divided by a factor 5. The form factors $F_i(Q)$ and the Co−Co distances $R_{ij}$ in eq 10 are taken from the literature.[33,36]

the use of the INS becomes essential in this case to get more detailed information on the exchange interactions.

We now refer to the structure of the $Co_5$ spin cluster in Figure 1d. The Co(II) ions 1 and 3 have an octahedral oxo-coordination formed by five oxo groups and one water molecule, whereas the Co(II) ion 2 is surrounded by six oxo groups. The Co(II) atoms 5 and 6 have a tetrahedral oxo-coordination. The edge-shared $CoO_6$ octahedra and the $CoO_4$ tetrahedra in Figure 1d share a common oxygen atom to form the pentamer.

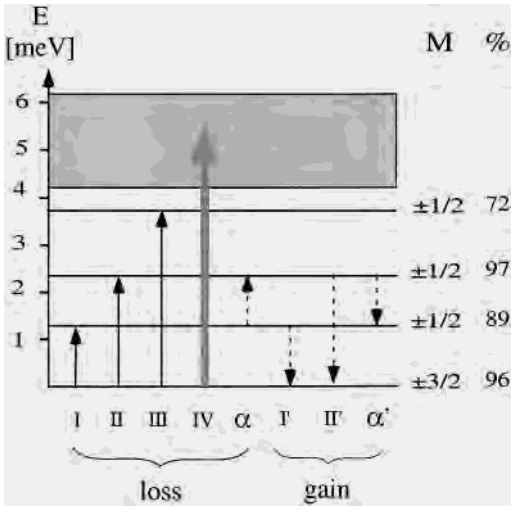


**Figure 7.** Experimentally determined ground-state splitting. Full arrows correspond to observed cold transitions I−IV, whereas the dashed arrows belong to hot transitions. The unresolved inelastic feature above 4.3 meV is indicated as a gray band. Each energy level is labeled according to the $M$ value associated with the basis functions having the leading contribution in the pentamer wave functions $\Psi_n$. This contribution, i.e., the sum of the squared coefficients in the linear combinations of eq 4, is given in the last column.

To understand the exchange coupling in the depicted pentamer, we first compare its structure with those of other related polyoxometalates containing Co(II) ions. The central fragment $Co_5$ formed by the Co(II) atoms 1, 2, and 3 and a W atom is identical to that of the isostructural polyoxometalate $Co_3$ (see Figure 1b,d). This polyoxometalate differs from the title compound in the replacement of the two tetrahedral Co(II) ions by diamagnetic Zn(II) ions. Moreover, the $Co_3$ fragment closely resembles the Co(II) tetramer present in the polyoxometalate $Co_4$ [37] (see Figure 1c). The Co(II)−Co(II) distances as well as the Co(II)−O−Co(II) angles change only slightly upon replacing one non-water-coordinated Co(II) atom by a W atom, as seen in Figure 1c,d. The mean Co(II)−O−Co(II) angles and the Co(II)−Co(II) distances are listed in Table 2. Thus, the exchange pathways along the oxo bridges are expected to be similar,

(36) Watson, R. E.; Freeman, A. J. *Acta Crystallogr.* **1961**, 27.
(37) Weakly, T. J. R.; Evans, M. H. T.; Showell, J. S.; Tourné, G. F.; Tourné, C. M. *J. Chem. Soc., Chem. Commun.* **1973**, 139.

**Table 2.** Co(II)−Co(II) Distances and the Mean Co(II)−O−Co(II) Angles for the Dimeric ($Co_2$), Trimeric ($Co_3$), Tetrameric ($Co_4$), and Pentameric ($Co_5$) Co(II) Spin Clusters[a]

| Co(II) ion number and coordination | | $Co_2$ | | $Co_3$ | | $Co_4$ | | $Co_5$ | |
|---|---|---|---|---|---|---|---|---|---|
| *i* | *j* | $R_{ij}$ [Å$^{-1}$] | α(*i*−O-*j*) [deg] | $R_{ij}$ [Å$^{-1}$] | α(*i*−O-*j*) [deg] | $R_{ij}$ [Å$^{-1}$] | α(*i*−O−*j*) [deg] | $R_{ij}$ [Å$^{-1}$] | α(*i*−O−*j*) [deg] |
| 1◆ | 2◆ | | | 3.192 | 99.81 | 3.164 | 97.14 | 3.192 | 99.81 |
| 2◆ | 3◆ | | | 3.170 | 98.61 | 3.192 | 97.62 | 3.170 | 98.61 |
| 1◆ | 5▲ | 3.660 | 125.96 | | | | | 3.380 | 117.29 |
| 2◆ | 5▲ | | | | | | | 3.313 | 114.58 |

[a] The values were calculated from the crystallographic data in refs 33, 37, and 38. The numbering scheme refers to the labeling in Figure 1. The type of oxo-coordination of the Co(II) ions is indicated by a diamond (octahedral) or a triangle (tetrahedral), as in Figure 1.

although the exchange anisotropy can change. The exchange pathway involving an octahedral and tetrahedral oxo-coordinated Co(II) ion connected through a common oxo group is also present in the Co(II) dimer encapsulated in the Keggin derivative $Co_2$ [38] (see Figure 1a). The Co(II)−Co(II) distance is reduced by 9%, and the Co(II)−O−Co(II) angle decreases from 126° to 117° in the pentamer compared to the dimer. The relevant Co(II)−O−Co(II) mean angles and Co(II)−Co(II) distances are also included in Table 2. Additionally the bridging oxygen atom in the pentamer is involved in two exchange pathways between an octahedral and a tetrahedral oxo-coordinated Co(II) ion, and we thus expect some changes in the exchange parameters.[27]

Taking into account that at low temperatures octahedral Co(II) ions can be described through an anisotropic spin $S = {}^1/_2$ (see above) and that tetrahedral Co(II) ions have a $^4A_2$ ground state, which can be described as a spin-only $S = {}^3/_2$,[35] we get the following effective spin Hamiltonian for the $Co_5$ moiety:[39]

$$\hat{H} = -2\sum_{i=x,y,z} J_{1i}[\hat{S}_{1i}\hat{S}_{2i} + \hat{S}_{2i}\hat{S}_{3i}] + J_{2i}[\hat{S}_{1i}\hat{S}_{5i} + \hat{S}_{2i}\hat{S}_{5i} + \hat{S}_{2i}\hat{S}_{6i} + \hat{S}_{3i}\hat{S}_{6i}] \quad (2)$$

In this model we are neglecting a possible zero-field splitting of the $^4A_2$ in the slightly distorted tetrahedral site, and the single-ion anisotropy of octahedral Co(II) ions is expressed in terms of the exchange anisotropy. Furthermore, the encapsulated $Co_5$ magnetic unit is well shielded from its surrounding and we can thus neglect any intercluster exchange interactions. In eq 2 the subscripts 1−3, 5, and 6 refer to the Co(II) ions in Figure 1d. $J_1$ is the exchange constant between the octahedral oxo-coordinated Co(II) ions, and the exchange constant between the octahedral and tetrahedral oxo-coordinated Co(II) ions is denoted as $J_2$. The operator in eq 2 does not commute with $\hat{S}^2$, the total spin of the cluster. Thus, it will mix the 128 $|S_{12}S_{123}S_{1235}SM\rangle$ basis functions, where $S_{12}$, $S_{123}$, and $S_{1235}$ are intermediate spin quantum numbers defined by the coupling scheme:

$$\vec{S}_{12} = \vec{S}_1 + \vec{S}_2, \quad \vec{S}_{123} = \vec{S}_{12} + \vec{S}_3, \quad \vec{S}_{1235} = \vec{S}_{123} + \vec{S}_5, \quad \vec{S} = \vec{S}_{1235} + \vec{S}_6 \quad (3)$$

The pentamer eigenfunctions will be given by appropriate linear combinations of these basis functions by

$$\Psi_n = \sum_{S_{12},S_{123},S_{1235},S,M} a_n(S_{12},S_{123},S_{1235},S,M)|S_{12}S_{123}S_{1235}SM\rangle \quad (4)$$

where $a_n(S_{12},S_{123},S_{1235},S,M)$ are the eigenvector coefficients of the cluster levels. For the energy calculation, the exchange Hamiltonian in eq 2 was expressed in terms of the irreducible tensor operators (ITO) of rank 2 and solved by means of a general numerical formalism that is valid for any spin cluster.[40] For an axial-anisotropic Hamiltonian ($J_{1x} = J_{1y}$ and $J_{2x} = J_{2y}$ in eq 2) $M$ remains a good quantum number in the pentamer wave functions. For a rhombic-anisotropic Hamiltonian ($J_{1x} \neq J_{1y}$ and $J_{2x} \neq J_{2y}$) basis functions with $\Delta M = \pm 2$ are mixed. This mixing is relatively small for a small rhombic term, and it is convenient to label the pentamer wave functions by the $M$ value associated with the basis functions having the leading contribution to the linear combination of $\Psi_n$ in eq 4.

We face a complex problem involving a large number of parameters, and therefore independent information can be useful to reduce the number of parameters in the fitting of the INS data. With this aim and bearing in mind the structural similarities of the magnetic $Co_5$ unit with the $Co_3$ and $Co_4$ units, we have fixed the values of the exchange parameters describing the ferromagnetic coupling between two octahedral Co(II) ions to those determined in these two cobalt clusters. The only parameters allowed to vary are then those associated with the antiferromagnetic exchange interaction $J_2$ because the oxygen-bridging angles change significantly in going from $Co_2$ to $Co_5$. Such a procedure can also be justified from the observation that the low-lying energy levels of the $Co_5$ spin cluster are much more dependent on the antiferromagnetic exchange interaction $J_2$ than on the ferromagnetic exchange interaction $J_1$. In parts a and c of Figure 8 the low-lying energy levels of the $Co_5$ spin cluster are plotted as a function of the exchange parameters $J_{2z}$ and $J_{1z}$, respectively. In the depicted axial-anisotropic situation we observe a much more pronounced dependence of the energy levels on the exchange parameter $J_{2z}$ than on the exchange parameter $J_{1z}$. Additionally, we also depict the behavior of the low-lying energy levels on the rhombic parameters $J_{2x}$ and $J_{1x}$ in parts b and d of Figure 8, respectively. We observe an additional variation of the low-lying energy levels on the parameter $J_{2x}$, whereas the dependence on $J_{1x}$ is completely negligible.

Thus, a first analysis of the data has been performed by fixing the parameters $J_{1x}$, $J_{1y}$, and $J_{1z}$ in eq 2 to those previously reported for $Co_4$. These parameters are all ferromagnetic with the following values:[29]

$$J_{1x} = 0.70 \text{ meV}, \quad J_{1y} = 0.43 \text{ meV}, \quad J_{1z}\ 1.51 \text{ meV} \quad (5)$$

Applying the effective Hamiltonian in eq 2 with $J_{2x}$, $J_{2y}$, and $J_{2z}$ as adjustable parameters to fit the energy levels of Figure 7, we get the best agreement with

$$J_{2x} = -1.24 \text{ meV}, \quad J_{2y} = -0.53 \text{ meV}, \quad J_{2z} = -1.44 \text{ meV} \quad (6)$$

(38) Baker, L. C. W.; McCutcheon, T. P. *J. Am. Chem. Soc.* **1956**, *78*, 4503.
(39) De Jongh, L. J.; Miedema, A. R. In *Monographs on Physics: Experiments on simple magnetic model systems*; Coles, Taylor and Francis: London, 1974; pp 1−269.
(40) Borrás-Almenar, J. J.; Clemente-Juan, J. M.; Coronado, E.; Tsukerblat, B. S. *Inorg. Chem.* **1999**, *38*, 6081−6088.

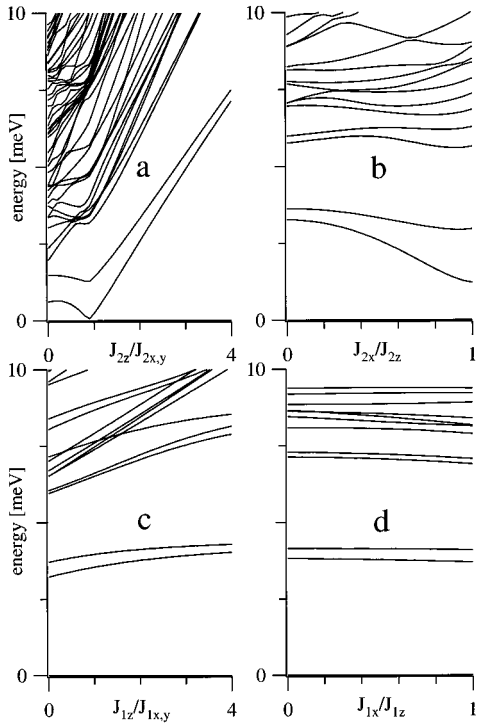


**Figure 8.** Energies of the low-lying energy levels of the $Co_5$ spin cluster as a function of $J_{2z}$ (a), $J_{2z}$ (b), $J_{1z}$ (c), and $J_{1x}$ (d). The remaining parameters in eq 2 were fixed to $J_{1x} = 1$ meV, $J_{1y} = 1$ meV, $J_{1z} = 2$ meV, $J_{2x} = -1$ meV, $J_{2y} = -1$ meV, and $J_{2z} = -2$ meV. The energy of the lowest level was chosen to be zero.

A second analysis of the data uses the ferromagnetic parameters $J_{1i}$ obtained for the $Co_3$ spin cluster:

$$J_{1x} = J_{1y} = 1.16 \text{ meV}, \quad J_{1z} = 1.73 \text{ meV} \tag{7}$$

The resulting set of parameters $J_{2i}$ is then

$$J_{2x} = -1.19 \text{ meV}, \quad J_{2y} = -0.53 \text{ meV}, \quad J_{2z} = -1.44 \text{ meV} \tag{8}$$

Both calculations reproduce in a satisfactory manner the experimental energy levels (see Table 1). These calculations also reproduce the band above 4.3 meV, where the density of cluster states increases beyond experimental resolution. We calculate seven energy levels between 4.3 and 6.5 meV. The total energy spread of the 128 cluster states is 19.3 meV.

The fact of getting similar agreements with the experiment in both calculations indicates that the actual splitting pattern of the ground state in the magnetic $Co_5$ unit is most sensitive to the size and anisotropy of the antiferromagnetic exchange constants ($J_{2i}$ in eq 2). This point has already been noted in Figure 8. Both calculations lead approximately to the same parameters $J_{2i}$.

Whereas an axial-anisotropic Hamiltonian with the parameters

$$J_{2x} = J_{2y} = -0.74 \text{ meV}, \quad J_{2z} = -2.24 \text{ meV} \tag{9}$$

was adequate to describe the exchange coupling in the Co(II) dimer,[27] only a rhombic-anisotropic model reproduces the energy splitting in the pentamer. This is not a contradiction because the differences in the bridging geometry between the dimer and the pentamer are significant (see Table 2).

An additional support of the validity of the above analysis is obtained from the magnetic properties. Both sets of parameters in eqs 5 and 6 and eqs 7 and 8 provide an accurate description of the low-temperature experimental data. The continuous decrease in $\chi T$ is well reproduced by a model that only considers as adjustable parameters the $g$ values of the two sites (Figure 3a). With both sets of exchange parameters we get an isotropic tetrahedral site with $g = 2.6$ and an anisotropic octahedral site with $g_{\parallel} = 7.9$ and $g_{\perp} = 3.5$. Isothermal magnetization versus field data at low temperatures are also well reproduced by the same parameters (Figure 3b).

We have previously shown for the polyoxometalate $Co_4$ that the hydrated octahedral Co(II) sites 1 and 3 in Figure 1c exhibit a larger spin anisotropy than the nonhydrated sites 2 and 4.[29] For the title compound such a precise determination of the $g$ factors is not possible solely from the magnetic data presented in Figure 3. We anticipate that an electron spin resonance experiment of a cobalt-codoped sample of $Na_{12}[Zn_3W(H_2O)_2(ZnW_9O_{34})_2]\cdot 46H_2O$ would allow a more thorough study of the spin anisotropies. Nevertheless, assuming the same spin anisotropies for the octahedral Co(II) sites 1−3 in Figure 1d, we obtain reasonable $g$ values. They compare well with earlier derived values for Co(II) sites with slightly distorted octahedral oxo-coordination, which are in the range $g_{\parallel} = 6.0-7.4$ and $g_{\perp} = 2.3-5.1$.[27,29]

A final test of the validity of the two solutions is provided by a comparison of intensities and $Q$ dependencies of the observed transitions with the theory. From this study, we get information on the nature of the eigenfunctions of the pentamer. These eigenfunctions $\Psi_n$ are obtained by diagonalizing the spin Hamiltonian in eq 2 with the parameter values in eqs 5 and 6. Using the parameters in eqs 7 and 8 leads to very similar wave functions. Therefore, in the present case this comparison will not allow us to discriminate between the two solutions. The $M$ values associated with the basis functions having the leading contribution to the pentamer eigenfunctions $\Psi_n$ are denoted in Figure 7. The label $M$ still has a physical meaning as seen by its relative weight of ~90% of the total wave functions. The complete wave functions $\Psi_n$ are used to calculate the relative intensities of transitions I−III and α, as well as their dependence on the scattering vector $\vec{Q}$. For pentamer transitions between the levels $|\Psi_n\rangle$ and $|\Psi_m\rangle$, the differential neutron cross section is given by[42]

$$\frac{d^2\sigma}{d\Omega\, dE} = C(Q,T)\sum_{\alpha,\beta}\left\{\delta_{\alpha\beta} - \frac{Q_\alpha Q_\beta}{Q^2}\right\}\sum_{i,j}\{g_i F_i(Q)\}\{g_j F_j(Q)\} \times \exp(i\vec{Q}(\vec{R}_i - \vec{R}_j))\langle\Psi_n|\hat{S}_i^\alpha|\Psi_m\rangle\langle\Psi_m|\hat{S}_i^\beta|\Psi_n\rangle \tag{10}$$

where

$$C(Q,T) = \frac{1}{4}\frac{N}{Z}\left\{\frac{\gamma e^2}{m_e c^2}\right\}\frac{k'}{k}\exp(-2W(Q,T)) \times \exp\left\{\frac{-E_{\Psi_n}}{k_B T}\right\}\delta(\hbar\omega + E_{\Psi_n} - E_{\Psi_m})$$

In eq 10 $k$ and $k'$ are the wavenumbers of the incoming and scattered neutrons, $\vec{Q}$ is the scattering vector, $\exp(-2W(Q,T))$ is the Debye−Waller factor, $g_i$ is the Landé factor, $F_i(Q)$ is the magnetic form factor, $\vec{R}_i$ is the space vector of the $i$th $Co^{2+}$ ion, $\gamma = -1.91$ is the gyromagnetic constant, and α and $\beta$ stand

(41) Silver, B. L. *Irreducible Tensor Operators*; Academic Press: New York, 1976.
(42) Marshall, W.; Lovesey, S. W. *Theory of thermal neutron scattering*; Clarendon Press: Oxford, 1971.

for the spatial coordinates *x*, *y*, and *z*. The remaining symbols have their usual meaning.

The matrix elements of $\hat{S}_i^{\alpha}$ and $\hat{S}_i^{\beta}$ are best evaluated by using ITO techniques.[41] Since our experiments are performed on a powdered sample with random orientation of the pentamer with respect to $\vec{Q}$, the cross section has to be averaged in $\vec{Q}$ space. In the case of a pentamer with anisotropic exchange, there is no closed analytical expression for the calculation of the INS cross section for a $|\Psi_m\rangle \rightarrow \langle\Psi_m|$ transition. We thus made use of a numerical formalism developed in ref 40, which is of general validity.

For a pure $M \rightarrow M'$ transition the following selection rule follows from eq 10:

$$\Delta M = 0, \pm 1 \tag{11}$$

Since *M* is still a relatively well-defined quantum number to characterize the cluster levels, the selection rule (eq 11) is still approximately valid. This allows us to assign all the observed cold inelastic transitions to allowed $\Delta M = \pm 1$ transitions and the hot transition α to an allowed $\Delta M = 0$ transition. The calculated relative intensities for transitions I−III and α are compared with the experimental ones in Table 1. The intensities of the first six rows (4.2 Å data) were integrated over the measured *Q* range from 0.28 to 2.50 $Å^{-1}$, and the intensity of transition I is scaled to 1. The relative intensities and their temperature dependence of transitions I and II and α are nicely reproduced by the calculation. The 7th to 10th row of Table 1 list the intensities of transitions II and III as obtained from the 2.79 Å data. They are integrated over the measured *Q* range (0.49−4.1 $Å^{-1}$), and the intensity of transition II is normalized to 1. The calculated intensity ratio of transition III to transition II is 3 times lower than the experimentally determined ratio. We ascribe this difference to experimental difficulties in determining the intensity ratio of transition III to transition II in the 2.79 Å data due to an underlying spurious intensity between 0 and 2 meV in the inset of Figure 5.

A comparison of the experimental and calculated *Q* dependencies of the INS intensities of transitions I, II, and III is depicted in Figure 6. In Figure 6a the observed *Q* dependencies for transitions I and II are depicted as full and open circles, respectively. They are closely reproduced by the calculated *Q* dependencies shown as full and dotted lines for transitions I and II, respectively. The calculated curves were normalized to the experimental intensity of transition I at $Q = 1.0$ $Å^{-1}$. Although both transitions are nominally $\Delta M = \pm 1$ transitions, they exhibit a completely different *Q* dependence. Whereas the calculated intensity of transition I shows a maximum, the intensity of transition II exhibits a minimum and vice versa. This is in perfect agreement with the experimental data, with the relative intensity of transition I or II following the same pattern. This different behavior has its origin in the differences in the intermediate and total spin quantum numbers $S_{12}$, $S_{123}$, $S_{1235}$, and *S* in the wave functions $\Psi_n$. The calculated *Q* dependence of transition III (Figure 6b) resembles that of transition I and nicely reproduces the experimental data. We interpret the match of experimental and calculated data in parts a and b of Figure 6 as a confirmation of our model and the derived parameters.

## 5. Conclusions

The title compound is an illustrative example of the complications arising from the interpretation of the magnetic behavior when dealing with both high-nuclearity clusters and transition-metal ions exhibiting a first-order single-ion anisotropy, such as Co(II). In analogy to the chemical construction of high-nuclearity clusters by assembly of smaller molecular fragments, one can build up the knowledge on the magnetic properties of a large magnetic cluster from the known magnetic properties of smaller subunits. Thus, the exchange network in the magnetic $Co_5$ cluster contains an octahedral−octahedral exchange interaction, which resembles that of the related $Co_3$ and $Co_4$ clusters, and a tetrahedral−octahedral exchange interaction, which resembles that of the $Co_2$ spin cluster. We show that the additional information on the exchange interactions derived from these simpler clusters, together with the high-resolution INS data on a fully deuterated sample of $Co_5$, allows a detailed description of the low-lying energy levels and exchange parameters of the cluster. In the present case, this has allowed us to identify the presence of two different exchange pathways having different signs and significant anisotropies. Still, it is important to note that even if several complementary techniques and independent information on related systems have been used, accurate new information has only been obtained on the antiferromagnetic tetrahedral−octahedral interaction. The ferromagnetic octahedral−octahedral interaction was shown to have a minor effect on the energy levels and magnetic properties of the cluster. This is so because the lowest energy levels of the cluster are determined to a large extent by the antiferromagnetic interaction. In fact, the exchange topology in this cluster is such that only the presence of an antiferromagnetic coupling, even a quite small one, is sufficient to stabilize those spin states with the lower *M* components, independent of the size of the ferromagnetic coupling. Finally, it is necessary to point out that this study has only been possible thanks to the great versatility of polyoxometalates in providing examples of largely insulated magnetic clusters of increasing nuclearities, common motifs, definite topologies, and high symmetries, compounds that can be easily deuterated in large amounts.

**Acknowledgment.** This work has been developed in the framework of the European COST ACTION 518 (Project: Magnetic Properties of Molecular and Polymeric Materials). Financial support by the European Union (TMR Network MOLNANOMAG, Contract HPRN-CT-1999-00012), the Spanish DGES (Grant PB960862), and the Swiss National Science Foundation is gratefully acknowledged.

IC001437A